Model of noncontact scanning force microscopy on ionic surfaces

Alexander I. Livshits and Alexander L. Shluger
Department of Physics and Astronomy, University College London, Gower Street, London WC1E 6BT, United Kingdom

Andrew L. Rohl
A. J. Parker Cooperative Research Centre for Hydrometallurgy, School of Applied Chemistry, Curtin University of Technology, P.O. Box U 1987, Perth, 6845 Western Australia, Australia

Adam S. Foster
Department of Physics and Astronomy, University College London, Gower Street, London WC1E 6BT, United Kingdom
(Received 9 July 1998)

We analyze the mechanisms of contrast formation in noncontact SFM imaging of ionic surfaces and calculate constant frequency shift scanlines of the perfect surfaces of NaCl, MgO, and LiF. The noncontact scanning force microscopy (SFM) operation is modeled by a perturbed oscillator using atomistic static and molecular-dynamics techniques for the force-field calculations. The electrostatic potentials of silicon tips contaminated by various atoms and that of a MgO tip are calculated using a periodic density-functional theory (DFT) method. Their analysis demonstrates that the presence of polar groups or chemisorbed species, such as oxygen atoms, makes the electrostatic forces acting on the surface ions from the Si tip one of the most important contributions to the image contrast. The $(MgO)_{32}$ cube model of the nanotip was found to be representative of a wide class of polar tips and used in the image calculations. The results of these calculations demonstrate that the contrast in noncontact SFM imaging of ionic surfaces is based on an interplay of the electrostatic and van der Waals forces. The main contributions to the contrast formation result from the interaction of the tip with the alternating surface potential and with the surface polarization induced by the electric field of the tip. The results emphasize the importance of the tip-induced relaxation of the surface ions in the tip-surface interaction and in image contrast. The noncontact SFM image of the Mg^{2+}-cation vacancy defect on the LiF surface is calculated using the same method. [S0163-1829(99)08803-7]

I. INTRODUCTION

Noncontact (NC) scanning force microscopy (SFM) (Refs. 1–6) is a rapidly developing branch of dynamic-force SFM,[7–9] which also includes the ''tapping'' mode recently discussed in Refs. 10 and 11, and other novel developments (see, for example, Refs. 12–14). NC-SFM has been successful in obtaining atomic scale images of Si(111),[2,3,5] InP,[4] TiO_2 (Ref. 15) and several alkali halides[6,16] in UHV. In this SFM technique, the cantilever oscillates with large amplitude and information regarding the surface properties is retrieved from analysis of frequency or amplitude changes of these oscillations due to the tip-surface interaction.[2,11,17] Although the first NC-SFM atomic scale images of Si(111) were obtained a few years ago,[2] reliable imaging has only been recently achieved, and the number of systems studied using this technique is still very limited. Part of the problem is that if the tip-surface interaction is too strong or changes sign, the cantilever oscillations may become unstable and the tip crashes into the sample surface. This implies that there are two conditions necessary for imaging: (i) there should be no strong long-range interaction (e.g., electrostatic forces due to the surface charging); (ii) even at the closest tip-surface separations, the tip should still be far enough from the surface to avoid strong adhesion. The first condition puts considerable restrictions on the surface preparation because all insulating surfaces cleaved in UHV are charged and require additional treatment to eliminate it. The second condition is technically difficult to fulfill since the tip-surface distance is unknown and the distance range of stable NC-SFM operation with measurable contrast is in many cases very narrow. Images obtained with this technique are deemed to be close to ''true'' atomic resolution due to several observations of stable point defects.[4,6,15] Therefore, a strong effort to improve the technique and to make it applicable to a wide range of insulators continues (see, for example, Refs. 14 and 18). Part of this effort is the development of a theoretical model that allows interpretation of experimental images.[17,19]

Theoretical modeling of NC-SFM includes two main components: (i) modeling of cantilever oscillations using known tip-surface forces; (ii) calculation of these tip-surface forces. The first problem has been considered in detail in conjunction with the ''tapping'' mode of SFM operation[10,11,20,21] and recently with respect to NC-SFM.[11,17,19] However, the chemical component of the tip-surface interaction that is responsible for adhesion, and in most cases the contrast formation, is difficult to quantify without atomistic modeling of representative systems. In particular, calculations[22] have demonstrated that the onset of chemical bonding between a dangling bond localized at the end of the tip and the dangling bonds on the adatoms of the Si(111) surface could contribute to the contrast formation. A detailed study of NC-SFM operation including an analysis of cantilever oscillations and the van der Waals and short-range forces has been performed by Giessibl.[17] Simple calculations of NC-SFM images of a model cubic lattice were performed in Ref. 23.

However, detailed mechanisms of contrast formation are still unclear. One of the reasons is related to the unknown structure of the end of the tip. Moreover, most of the experimental papers admit that NC-SFM is prone to instabilities resulting in tip contamination due to contact with the surface leading to variations of the atomic structure of the tip apex.[4,5,16] Apart from purely technical reasons, these instabilities in NC-SFM operation could result from the onset of adhesion avalanche of the surface or tip atoms.[24–28] However, the role of this effect in NC-SFM has not been properly understood. The analysis of the NC-SFM image of Si(111) made in Ref. 5 led the authors to suggest that the image contrast could be due to variations in the relaxation of the outermost surface atoms due to their interaction with the tip. The importance of relaxation of surface ions in contact mode SFM has been demonstrated in Refs. 29–31. As we will see below, this is also one of the key effects that determine the image contrast in NC-SFM on ionic systems.

In this paper, we study the mechanisms of NC-SFM imaging of ionic surfaces, such as alkali halides and MgO. The alkali halides are easy to cleave and in many respects they have been treated as model insulators in SFM studies.[1,6,32,33] MgO is a prototype oxide with many applications as a substrate and in catalysis; however, flat surfaces of MgO are much more difficult to prepare. It has the same structure as alkali halides, which allows useful comparison between the two materials. Our discussion is focused on three key aspects: First, we discuss a tip model and simulation of NC-SFM operation. Then the role of avalanche adhesion in the tip-surface interaction is considered in conjunction with the stability of NC-SFM operation. Finally, we analyze the mechanisms of contrast formation and resolution through modeling NC-SFM images of perfect surfaces and of a point defect at the LiF surface.

The interactions between tips and surfaces at large distances important in NC-SFM on ionic crystals include the van der Waals and electrostatic contributions.[27,34] The latter includes the Coulomb interaction between the tip and surface, contributions due to tip and surface polarization and is mostly responsible for the image contrast. Our approach is to consider one tip and several surfaces which have the same structure but differ in terms of their interaction with the tip by two parameters—effective ionic charge and lattice constant. LiF and MgO have very similar lattice constants but different charge; LiF and NaCl have similar charge but different lattice constants. In Sec. II we discuss the model of NC-SFM operation and the tip structure. The methods used for calculating forces between the tip and the surface are discussed in Sec. III, the results of our modeling are given in Sec. IV, and discussed in Sec. V.

II. MODEL OF NC-SFM

In NC-SFM, a cantilever oscillates with large amplitude near its resonance frequency, and, by applying special control strategy, the tip is held in the attractive part of the interaction even at the closest tip-surface distance. When the tip is approaching the surface, this interaction affects the cantilever oscillations and the resulting frequency shift as a function of lateral tip position, averaged over many cantilever oscillations, can be determined. An image is created by scanning the surface in the xy plane, e.g., at constant cantilever amplitude and keeping the frequency shift constant by controlling the equilibrium position of the cantilever h.[3,6,16] Other modes, such as constant reduction of oscillation amplitude, are also used.[5] For interpretation of these images, a knowledge of the relationship between the tip-surface forces and the detected parameters of the cantilever oscillations is required. This issue has been treated in recent publications.[2,11,17] If the tip enters the repulsive part of the interaction and probes elastic surface properties, called ''tapping mode,'' the tip-surface force can be linearized and the equations describing cantilever oscillations can be solved analytically.[21] When the attractive part of the interaction is probed, the tip-surface forces are strongly nonlinear and the equations of motion of the cantilever can be solved numerically[11] or using perturbation theory.[17] In this section we discuss the numerical method used in this paper to describe the cantilever oscillations for given tip-surface forces. Combining this with the model of the tip structure comprises our model of NC-SFM.

A. Model of cantilever oscillations

The oscillations of a cantilever driven by an external force F_{ext} in a force field $F(z)$ can be described by the equation of motion:

$$\ddot{z}+\frac{\omega_0^2}{k}\,\alpha\dot{z}+\omega_0^2 z-\frac{\omega_0^2}{k}\,F(z+h)=F_{\text{ext}}\frac{\omega_0^2}{k},$$

where $\omega_0=2\pi f_0$ and k are the resonance frequency and the spring constant of the cantilever respectively, α is a damping coefficient, and h is an equilibrium position of the cantilever above the surface in the absence of the tip-surface interaction. In this paper, we are concerned with interpretation of stable NC-SFM images obtained at constant amplitude and constant frequency change[6,16] in UHV. Therefore, we assume that any damping is completely cancelled by the external force, which has a frequency equal to the eigenfrequency of cantilever vibrations, and that $F(z)$ does not depend on time. Then solutions for the cantilever oscillations can be found from the more simple equation:

$$\ddot{z}+\omega_0^2 z-\frac{\omega_0^2}{k}\,F(z+h)=0. \tag{1}$$

As discussed below, the condition $F(z)\neq F(z,t)$ holds if we assume that stable imaging does not involve trapping of the tip and surface ions by the surface or the tip. If the characteristic times of ionic jumps between the tip and surface are comparable to the cantilever oscillation period, the above condition is not valid.

As the cantilever motion is periodic, we can search for a solution of Eq. (1) in the form of a Fourier series for the oscillator coordinate z:

$$z(t)=\sum_{n=0}^{\infty} A_n\cos(2\pi f n t). \tag{2}$$

It is convenient to use a dimensionless time $\tau=2\pi ft$ and frequency $\Omega=f/f_0$. Substituting Eq. (2) into (1) and using these new notations, the following equation of motion is obtained:

$$\sum_{n=1}^{\infty}[1-(n\Omega)^2]A_n\cos(n\tau)+A_0-\frac{1}{k}F(z+h)=0. \quad (3)$$

To find Ω, A_n, $n=0,2,...,\infty$, for given A_1, h, and $F(z)$, we multiply Eq. (3) by $\cos(j\tau)$ and integrate the result over the period of main frequency $\tau=[0,2\pi]$. In this way, a system of nonlinear equations for A_n, $n=0,2,3,...,m$, is obtained, which is approximate for finite m:

$$A_0-\frac{1}{2\pi k}\int_0^{2\pi}F(z+h)d\tau=0,$$

$$A_n-\frac{\int_0^{2\pi}F(z+h)\cos(n\tau)d\tau}{\pi k-\pi kn^2+\frac{n^2}{A_1}\int_0^{2\pi}F(z+h)\cos(\tau)d\tau}=0. \quad (4)$$

If we designate the left-hand side of Eq. (4) as $\phi_n(A_0,A_2,\ldots)$, one can rewrite this system of equations in a more compact way:

$$\phi_n(A_0,A_2,\ldots)=0,\ \ n=0,2,3,...,m,$$

and solve it using a modified Newton method. First, we set all A_i except A_1 to zero. For each iteration the values of increments $\{\Delta A_i\}$ can be obtained by solving the equation

$$\frac{d\phi_n}{dA_0}\Delta A_0+\sum_{j=2}^{m}\frac{d\phi_n}{dA_j}\Delta A_j=-\phi_n. \quad (5)$$

However, the iterative procedure built in this way is often divergent. Therefore the increments $\{\Delta A_i\}$ obtained from Eq. (5) are used only to find a search direction. The absolute values of the increments $\{\Delta A_i\}$ are calculated by minimizing the residual function

$$\Phi(\lambda)=\sum_{i=0}^{m}\phi_i^2\{(A_i)_k\}, \quad (6)$$

with respect to the parameter λ, where

$$(A_i)_k=(A_i)_{k-1}+\lambda\Delta(A_i)_{k-1}.$$

In the latter equation, k stands for the iteration number and i is the index of the unknown coefficient. Finally, the frequency of cantilever oscillations in the presence of the interaction, Ω, is obtained as

$$\Omega_2=1-\frac{1}{\pi kA_1}\int_0^{2\pi}F(z+h)\cos(\tau)d\tau. \quad (7)$$

We should note that similar formulas were obtained in Ref. 17 using perturbation theory and a particular expression for the force $F(z)$.

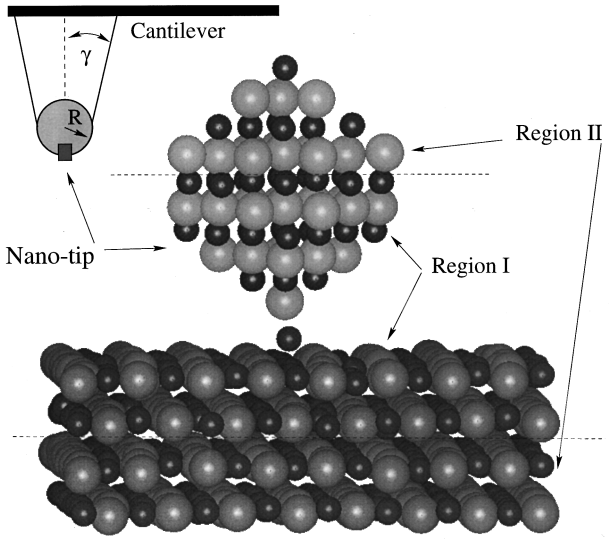

FIG. 1. A schematic of the SFM tip and a snapshot of a representative atomic configuration of the MgO nanotip interacting with the LiF surface. The tip is modeled by a cone with angle γ and a sphere of radius R at the end. The nanotip is embedded at the bottom of the sphere. Note the strong displacement of the Li ion from the surface towards the tip.

B. Tip model

To calculate the van der Waals interaction between the tip and the surface, a knowledge of the tip macroscopic shape is required. Expressions have been derived for the van der Waals interaction between macroscopic tips of different shape and plane surfaces as a function of the Hamaker constant, geometric parameters of the tip and the distance between the end of the tip and the surface plane (see, for example, Refs. 17, 35, and 36). However, the latter distance is not well defined on an atomic scale. To avoid significant errors at short distances and at hard tip-surface contact, the van der Waals interaction between the tip and surface atoms in the contact area should be considered atomistically. The ''chemical'' forces between these atoms and the surface atoms are largely responsible for the image contrast. Therefore, the tip in our calculations is divided into two parts (see Fig. 1): (i) a macroscopic part, and (ii) an atomistic part at the end of the tip (nanotip). The macroscopic tip is modeled by a cone with a sphere of radius R embedded at the end, as shown in Fig. 1. However, a reliable model of the nanotip is much more difficult to generate.

In our previous SFM modeling[27,29–31] we used a MgO cluster as a nanotip model. It is a good model of a hard oxide tip, which has the important advantage that there are reliable interatomic potentials for the interaction between MgO and alkali halides and other oxides. On the other hand, most of the commercial cantilevers are microfabricated from silicon and are covered by a native oxide layer. This layer is thought to be removed in some experiments by sputtering with Ar^+ ions. However, the chemical structure and geometry of the very end of the tip is practically impossible to control. Therefore, any nanotip model can only be justified based on circumstantial evidence and on comparison of calculated images with experiment. Some factors that may help in the generation of a realistic model of the nanotip structure are as

follows: the silicon nanotip should display the characteristic features of the most stable Si(111) (7×7) surface; it may have some residual oxide layer or oxygen adsorbed on it; it can be contaminated by residual hydrogen or water from the vacuum chamber; and it can also be contaminated by the surface material.

To check the feasibility of a simple MgO tip model, we have studied silicon tips with various contaminants. The most important component of the tip-surface interaction with ionic surfaces at long distances in NC-SFM is the electrostatics. Therefore, as a criterion for comparison of different tips, we used the gradient of the electrostatic potential produced at low-coordinated tip sites that are likely to serve as probes. The full details of these calculations will be published elsewhere.[37] Here we present a brief summary of the results relevant to this study.

The calculations were made using the periodic DFT method based on the Car-Parrinello technique,[38] in which the total energy of the system is minimized with respect to the plane-wave coefficients of the occupied orbitals. We used the VASP code[39,40] where the ''soft'' Vanderbilt pseudopotentials[41,42] are implemented. The method employs the generalized gradient approximation (GGA) functional of Perdew and Wang[43,44] known as GGA-II. The calculations were performed for a periodic arrangement of clusters separated by large vacuum gaps and using a periodic slab model for surface calculations.

To have a practical tip model for the *ab initio* calculations of the tip-surface interaction, we assumed that the adatoms, which are the most protruding of the surface atoms, are most likely to serve as the probe species. A surface adatom can be well represented by a Si_{33} cluster[45] or by a smaller Si_{10} cluster.[22,46] To check whether this really is a representative model for the Si(111) surface, we have calculated the geometric and electronic structure, and the electrostatic potential for the (5×5) surface reconstruction.[22] The latter is the smallest model containing the same basic structural features as the (7×7) reconstruction.[47] The electrostatic potentials near the adatom on the Si(111) surface and that produced by the Si_{10} cluster are shown in Figs. 2(a) and 2(b). As one can see, despite the surface polarization by the low-coordinated atoms, the electrostatic potential in both cases decays very quickly. We should note at this point that since the electrostatic potential was calculated in the periodic model, it is defined only up to a constant that is different for different systems and periodic cells. Therefore, strictly speaking, meaningful comparison can be made only in terms of potential gradients, although in some cases the absolute values of the potential are also well defined.

To compare different plausible tip models we also considered Si tips contaminated by several species. In particular, water is known to dissociate to the hydrogen atom and OH radical on the Si surface.[48] Therefore, we considered the silicon tip with these species adsorbed on the adatom site, which is known to be the most reactive surface site.[49] To model the residual oxide and silicon tip contamination by oxygen due to contact with an oxide surface, an oxygen atom was adsorbed on the tip adatom. Test calculations for the Si_{33} and Si_{10} clusters with adsorbed species gave very similar results. Therefore, the electrostatic potentials calculated for the Si_{10} cluster only are presented in Figs. 2(c)–2(e).

One can see that the adsorption of the hydrogen atom does not significantly affect the tip potential. However, the adsorption of a polar OH group produces a much more extended potential which spreads on about 2 Å from the terminating H atom [Fig. 2(d)]. The strongest electrostatic potential is produced by the tip with the oxygen atom adsorbed on the adatom site [see Fig. 2(e)], which is caused by the strong electron density flow from the nearest silicon atoms to the oxygen. Comparison with the electrostatic potential produced by the oxygen corner of the $(MgO)_{32}$ cube shown in Fig. 2(f) demonstrates strong similarity between the two. The effective ionic charges in the cube are close to $\pm2\ |e|$ (e is the electron charge) and therefore the potential at the cube corner should be stronger. At distances exceeding 3.0 Å from the corner ion, the absolute values of the potential are affected by interactions with other periodically translated cubes. Nevertheless, one can see that the potential gradients produced by the Si_{10}-O cluster and the MgO cube corner are similar.

These results demonstrate that the Si and Si-H tips are unlikely to have a strong electrostatic interaction with ionic surfaces. The electrostatic contribution in this case may come from the polarization of the tip by the surface electric field.[50] However, the presence of polar groups or chemisorbed species, such as oxygen atoms, makes the electrostatic forces acting on the surface ions from the tip much stronger. As we will see below, gradients of these forces can, in some cases, be measured at the tip surface separations as large as 4.5–6.0 Å, which is very important for really nonintrusive tip-surface interaction. In this distance range, the $(MgO)_{32}$ cube model of the nanotip is representative of a wide class of polar tips and will be used throughout further discussion. This allows us to obtain reliable results using the atomistic simulation techniques described in the next section.

III. CALCULATION OF FORCES

Tip-surface forces have been reviewed in several publications.[26,51–54] Some of them, such as the long-range electrostatic forces due to surface charging after cleavage and patch charges, are in many cases so strong that high-resolution imaging is impossible. This problem is most acute for alkali halides and oxides cleaved in vacuum. It can be solved by heating the samples or by using thin films grown on metallic substrates. We assume that if high-resolution imaging is achieved, these long-range electrostatic forces can be neglected. In UHV, the forces that are mostly responsible for the image contrast are determined by the ''chemical'' interactions between the tip apex and the surface atoms. To treat these interactions, we employ classical static atomistic and molecular dynamics techniques. The molecular-dynamics technique allows us to take into account the effect of temperature on the dynamics of ions especially in the region close to the avalanche adhesion where the barriers for ionic jumps are small. The schematic model used in our calculations is shown in Fig. 1. The nanoasperity at the end of the tip and several upper surface layers are treated atomistically as described below.

For static calculations we employed the atomistic simulation technique[56] implemented in the MARVIN computer code, which is fully described in Refs. 27 and 55. The tip and

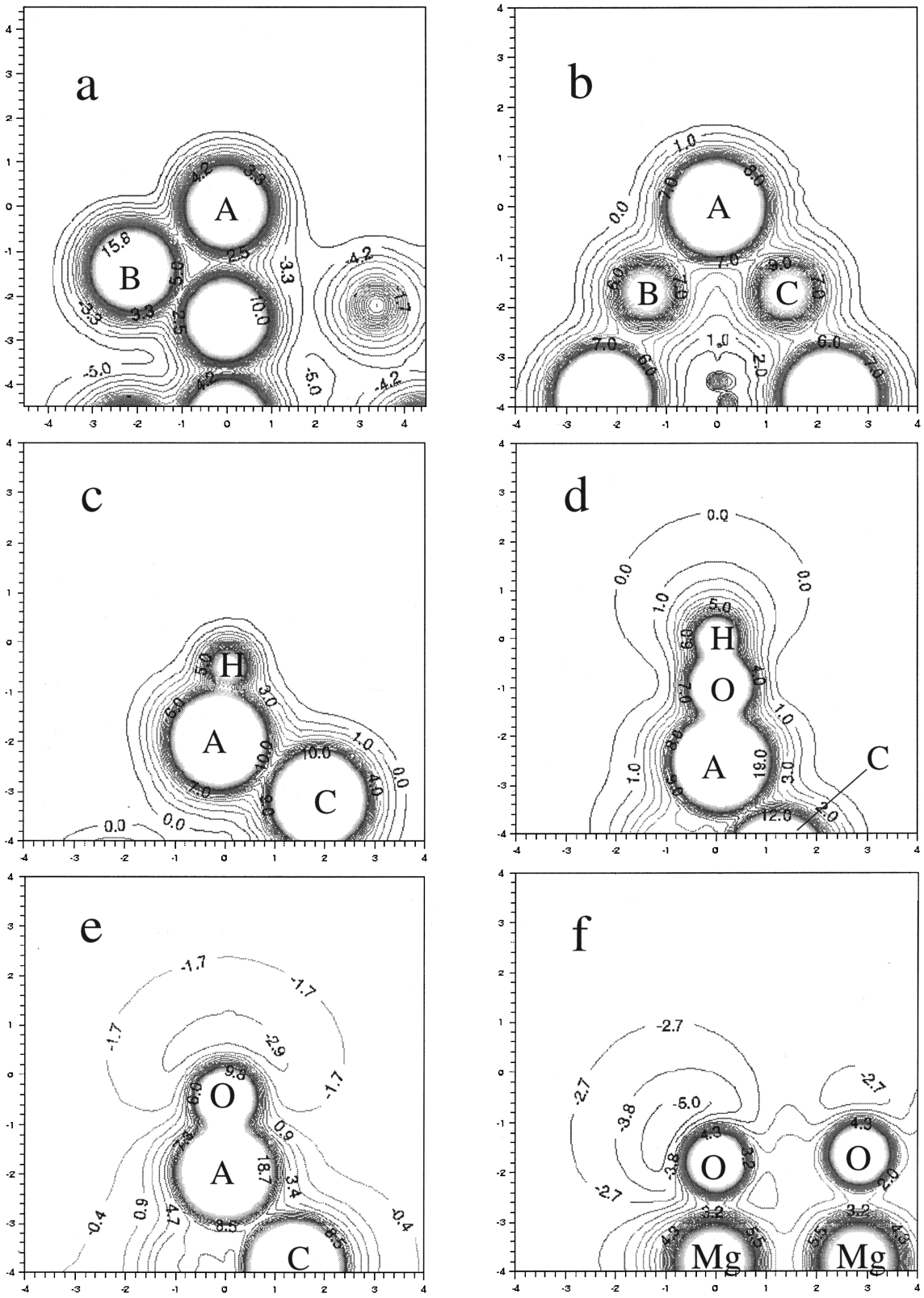

FIG. 2. Sections of the electrostatic potential calculated for several silicon structures and the $(MgO)_{32}$ cube using the periodic DFT method. The scale on the axes is in angstroms and the units of the contours are in eV. *A*, *B*, and *C* represent equivalent atoms in the Si surface and Si_{10} cluster; atom *A* is the adatom. (a) The adatom site on the reconstructed Si(111) (5×5) surface; (b) the adatom modeled by the Si_{10} cluster; (c) the hydrogen atom adsorbed on the Si adatom in the Si_{10} cluster; (d) the OH radical adsorbed on the Si adatom in the Si_{10} cluster; (e) the oxygen atom adsorbed on the Si adatom in the Si_{10} cluster; (f) the oxygen corner of the $(MgO)_{32}$ cube; the potential is shown in the plane that includes the ⟨111⟩ cube axis through the oxygen tip ion. Note that in (b) the section is made in the symmetry plane, whereas in (c)–(e) the section is through atoms *A* and *C*, and the adsorbed species.

surface ions were treated by the ionic model. Electronic polarization of ions is incorporated via the Dick-Overhauser shell model,[57] in which an ion is considered to consist of a core connected by a harmonic spring to a massless shell, i.e., the ion consists of two separate particles. The total charge of the ion is split between the core and shell. This partition and the harmonic spring constant determine the magnitude of the ionic polarization. All the ions in these calculations had their full formal charges and only polarization of the anions F^-, Cl^-, and O^{2-} was taken into account. To calculate the electrostatic energy, we have exploited the algorithm of Heyes, Barber, and Clarke.[58] Buckingham two-body potentials were used to represent the non-Coulombic interactions between the ions. The parameters of these potentials are described in Refs. 27, 59, and 60. They are derived for ions in crystals and in small clusters, and thus effectively averaged over the surface sites of different coordination.[27] We have used quantum-mechanical calculations to check whether the electronic configurations of the ions in the contact area remain the same as those used in the parameterization of the potentials.[28,30]

The nanotip and the upper surface layers are each split into two regions (I and II), as discussed in Refs. 27, 29, and 55. The region I ions are relaxed explicitly until there is zero force on each of them, while those in region II are kept fixed to reproduce the potential of the bulk lattice and the rest of the tip on region I ions. The simulation cell shown in Fig. 1 has planar two-dimensional periodic boundary conditions parallel to the interface. To model a single tip at the surface, the interaction between the periodically translated nanotips and the interaction between the areas of surface deformation should be small. This is ensured by using a large surface area. In the present calculations, the surface region I contained three planes of 100 ions, which were allowed to relax. The surface region II contained five planes of frozen ions.

In the MD calculations, the surface was modeled by a large cluster and the whole system was composed of 2704 ions. The tip and the surface were divided into three regions: in region I, the tip and surface ions move according to Newton's equations of motion; the surface and the tip ions in region II formed a thermal bath and were treated as being in thermodynamic equilibrium at room temperature; region III includes the ions of the upper part of the nanotip and the bottom and the sides of the cluster simulating the surface, which are kept fixed. The interactions between ions were calculated using the same pair potentials as in the static calculations;[27] however, all ions were treated as nonpolarizable.

To run the simulations we used the DL_POLY 1.1 package of molecular-dynamics routines[61] modified for SFM simulations as discussed in Ref. 30. The Berendsen algorithm[62] with an equilibration time constant of 10^{-12} s was used to keep temperature constant in the region II. The forces on the tip were calculated as the sum of forces on all the particles averaged over a time period of 10^{-12} s. To integrate the Newton equations, the Verlet ''leap-frog'' scheme with a time step of 2×10^{-15} s was employed.

IV. RESULTS

We start by discussing factors that may affect the stability of NC-SFM operation. Then the calculated images of the perfect LiF, NaCl, and MgO surfaces are presented, and finally we consider an image of an impurity defect at the surface of LiF.

A. Role of avalanche adhesion in the stability of NC-SFM operation

One of the main drawbacks of contact SFM which the NC mode strives to overcome is a so-called jump-to-contact effect (see, for example, Refs. 52 and 63). It is caused by the strong van der Waals force and other attractive forces between the tip and sample (e.g., long-range electrostatic forces due to surface charging). In contact SFM, when the derivative of the sum of these forces towards the surface exceeds the cantilever spring constant, the tip would pierce the surface in an uncontrolled way. However, this effect can be prevented in NC-SFM due to the cantilever oscillation. To achieve this, one should use cantilevers with large spring constants and apply large oscillation amplitudes so that the cantilever bending force always exceeds the sum of the attractive forces. These stability criteria for NC-SFM operation based on the jump-to-contact effect were considered by Giessibl.[17] For common operating parameters, such as a cantilever spring constant of 30 N/m and cantilever vibrations of amplitude 10 nm, the attractive force that may lead to jump-to-contact needs to be greater than 300 nN. Such forces may occur, for example, due to the strong surface charging when one tries to image alkali halides or oxides cleaved in vacuum. Otherwise the tip-surface forces are much smaller. Nevertheless, instabilities are often observed while a periodic image is being routinely collected. They lead to tip crushing or contamination by the surface material.[4,5,16] Since tip modifications may lead to image inversion and distortion, this makes atomistic interpretation of images, and especially those of ''point defects,'' unreliable. Therefore it is important to study and eliminate other possible reasons for instabilities in NC-SFM operation.

An empirical condition widely used for attaining stable NC-SFM operation is to work on the attractive part of the tip-surface interaction curve.[3] If the tip suddenly encounters a much less attractive or a repulsive interaction, the SFM electronics assumes that the cantilever should move closer to the surface searching for stronger attraction. This purely technical drawback often leads to the tip crashing into the surface. It can be provoked by surface defects, adsorbed species or by fluctuations in the amplitude of the cantilever vibrations.

Are there any other more ''physical'' effects that may lead to the tip touching or crashing into the surface? In particular, to be able to resolve different ions, the smallest tip-surface separation should be comparable to interatomic distance. At such distances an avalanche adhesion of the surface ions on the tip (and vice versa) may become important.[28] This effect is similar to avalanche adhesion of solid surfaces, which was first demonstrated for metals.[25] Its mechanism for metallic tips and surfaces was considered in Refs. 26, 51, and 64–67. For ionic materials, it was discussed in Ref. 28. The occurrence of instabilities of the surface and tip ions or atoms strongly depends on the tip and surface chemical structure and the tip-surface distance, and is relevant to our discussion of NC-SFM operation in two ways. First, the instability means that at some critical tip-surface distance,

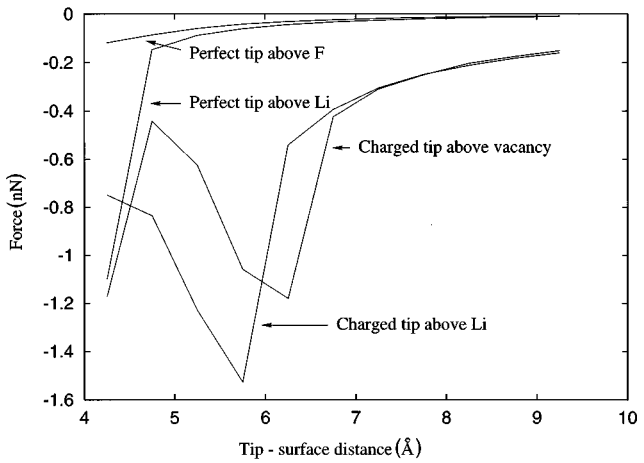

FIG. 3. The force vs distance curves calculated above different sites of the MgO tip interacting with the ⟨100⟩ LiF surface with and without an adsorbed surface Li ion.

the surface ions strongly displace from their sites causing an abrupt change in the tip-surface interaction.[27,64,68] Although the change in the force due to this effect may be often just 0.3–1.0 nN, the force gradient is of the order of 10–30 N/m. Second, if this or a smaller tip-surface distance is the turning point of the tip oscillations, some surface ions may be trapped by the tip, changing the tip-surface interaction even more strongly. The assumption of the stationary force-field $F(z,t)=F(z)$ may become invalid if the frequency of these tip modifications is comparable to the period of the cantilever oscillations, resulting in these oscillations becoming very complex. Can these effects affect the cantilever oscillations in any significant way?

To answer this question, we first considered the interaction of the MgO tip with the LiF surface. Our previous calculations[27,28] have demonstrated that if the oxygen terminated MgO tip approaches the LiF surface above a Li ion closer than approximately 4.5 Å, the single stable position of the Li ion is between the tip and the surface at approximately 1.2 Å above the surface (see Fig. 1). This is due to formation of a single potential well for the Li between the tip and the surface, as discussed in Ref. 28. This effect leads to a significant increase in the tip-surface attraction. This can be seen in Fig. 3, which shows the force curves calculated using the molecular-dynamics technique. Note that the distance referred to in Fig. 3 and in further discussion throughout the paper is measured between the ideal position of the oxygen ion at the end of the tip and the ideal surface plane. We calculated the changes in the amplitude of the cantilever vibrations A_1 and in the displacement of the equilibrium position of the oscillation A_0 induced by this force change. Both values appeared to be less than 0.1 Å, suggesting that this effect cannot immediately affect the cantilever motion. However, as the tip moves back from the surface, two things may happen:[28] (i) a single Li ion can be trapped by the tip; and (ii) adsorption of a Li ion on the tip may initiate formation of a string of ions stretching out of the surface or even a neck.

Next, we assumed that a Li ion is trapped by the tip and calculated the force curves above the vacancy remaining on the surface and above another Li surface site, which are also shown in Fig. 3. We expected to see strong repulsion above the Li site. This would signal that the tip charging may lead to the tip crashing into the surface because the electronics would follow the attraction scenario. However, contrary to our expectation, both force curves show Coulomb attraction at long distances with a clear sign of instability at approximately 6 Å above the surface (note that this is the distance between the tip oxygen ion and the surface plane). Detailed analysis of molecular dynamics has revealed that the adsorbed Li ion is in fact very mobile on the tip and adjusts its position in response to attraction from the surface F ions. This, along with the strong surface polarization by the charged tip, produces the attraction at large distances. At approximately 6 Å, the effective distance between the adsorbed Li ion and the surface plane is approximately 4.5 Å and one of the F ions becomes unstable in its site and strongly displaces towards the Li ion on the tip. We did not follow this scenario further in this work, but, as was demonstrated in our recent paper,[28] this may be a beginning of the formation of a long chain as the tip and the surface separate again. Using the force curves for the charged tip, we have calculated the parameter A_0, which gives an additional displacement of the tip towards the surface due to the shift of its equilibrium caused by the tip-surface interaction. The marginal value of $A_0 \approx 0.3$ Å obtained in both cases suggests that the tip is not likely to enter the repulsive part of the interaction. These results lead us rather to suggest that the initial tip contamination can develop into a neck formation or adsorption of a cluster of the surface material onto the tip, which can eventually lead to the tip crashing into the surface.

B. Calculation of surface images

To study the mechanisms of contrast formation in NC-SFM, ''constant $\Delta\omega$'' scanlines for the LiF, NaCl, and MgO surfaces were calculated using the following method. For each surface, a number of force versus distance curves were first calculated using the classical atomistic simulation techniques described above. The calculations were made on a mesh (x,y) above a number of surface points in the distance range $z=3.5-6.3$ Å. This provides the same asymptotic behavior for all curves for the same crystal which is determined by the atomistic contribution to the van der Waals interaction and the surface polarization by the tip. The calculated points were then approximated analytically by a sum of several inverse powers. The asymptotic behavior of the tip-surface interaction potential was always determined by the z^{-3} term. The van der Waals interaction between the macroscopic part of the tip and the surface was calculated using a model of a conical tip with the half-angle $\gamma=30°$ and a sphere of radius R embedded at the end (see Fig. 1). The expressions for the forces between such a tip with a semi-infinite surface are published in Ref. 36. The Hamaker constant was fixed in all calculations equal to 1.70×10^{-21} J as was found for the MgO/MgO interaction in Ref. 69. The strength of the van der Waals interaction was changed by using different tip radii R.

These calculated analytical expressions for $F(z)$ were then used in Eqs. (1)–(7) to calculate the set of stationary frequencies $f(h)$ and the corresponding amplitudes A_i for different equilibrium positions of the cantilever above the surface, h, and for each surface mesh point (x,y). In these calculations, the value of the cantilever eigenfrequency f_0

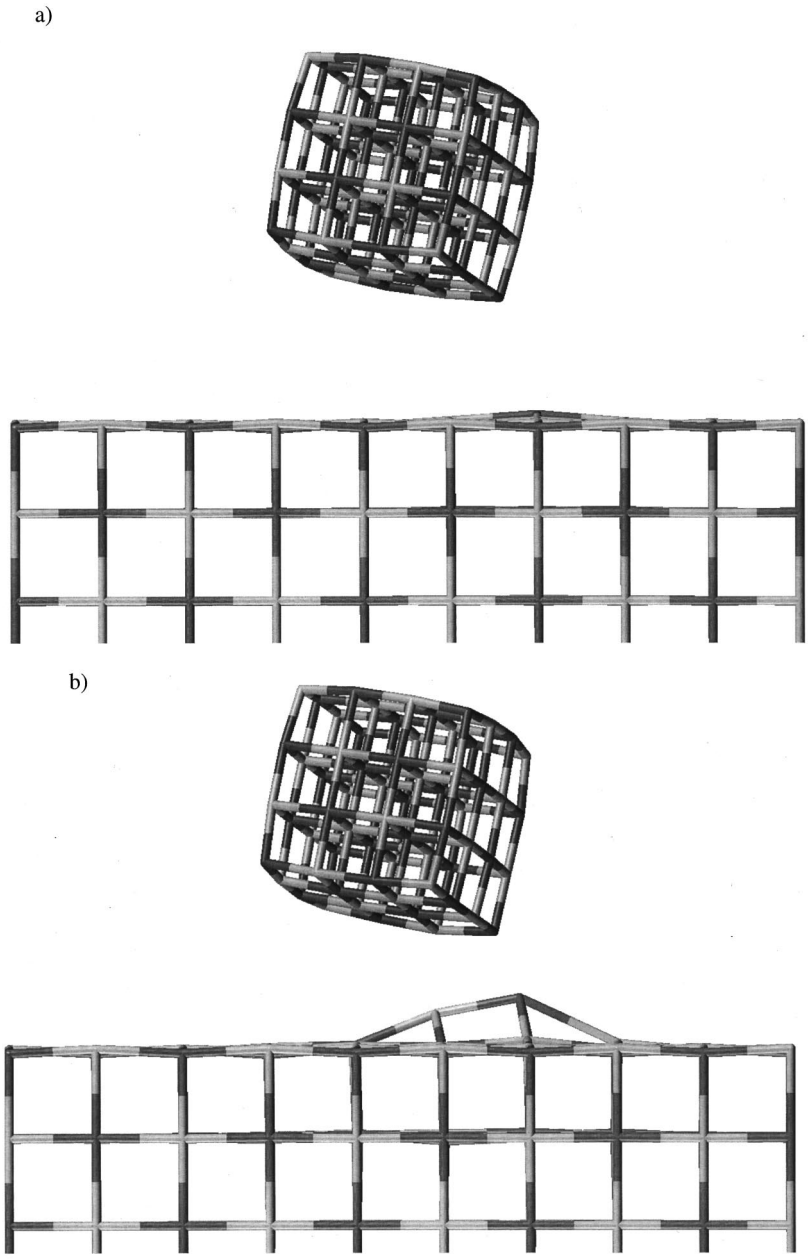

FIG. 4. The snapshot configurations of the MgO nanotip interacting with the NaCl surface. (a) corresponds to the tip-surface distance approximately 4.2 Å just before, and (b) to the distance 4.1 Å and the configuration just after the instability of the surface Na ion has occurred. Note the strong displacements of the surface ions in both cases.

was equal to 168 kHz and the amplitude A_1 was 130 Å, as in the experiments.[6] In all cases, the amplitudes A_i ($i=2,3,...,20$) were found to be at least two orders of magnitude smaller than A_1. The scanlines were then calculated as $h(x,y)-A_1$ for a given constant $\Delta f=|f-f_0|$ and tip radius R.

The calculations for the MgO and NaCl surfaces were made using the static atomistic simulation technique employed in the MARVIN code. The MgO tip was oriented by one of its oxygen corners to the surface and the direction of the cube diagonal through this ion with respect to the surface was chosen in an arbitrary way, resulting in a blunter tip than that used in the LiF simulations (see Fig. 4). The tip was moved along the ⟨100⟩ surface axis directly above the row of the surface ions for several lattice constants with the lateral step of 0.4 Å and the vertical step equal to 0.1 Å. The potential energy curves $E(z)$ were calculated at each lateral tip position. The calculated points were approximated by analytical expressions and the scanlines shown in Figs. 5 and 6 were obtained as discussed above.

A more complex study was performed for the LiF surface. In this case, our ultimate aim was to obtain an image of a point defect, but one scanline is not enough to estimate the extent of defect induced perturbation. For comparison, we first calculated the full image of the perfect surface using the ideal tip orientation by the cube diagonal perpendicular to the surface shown in Fig. 1. The $F(z)$ curves were calculated directly using the molecular-dynamics technique at room temperature on the mesh of nine symmetry surface points. Some of the $F(z)$ curves corresponding to the chemical com-

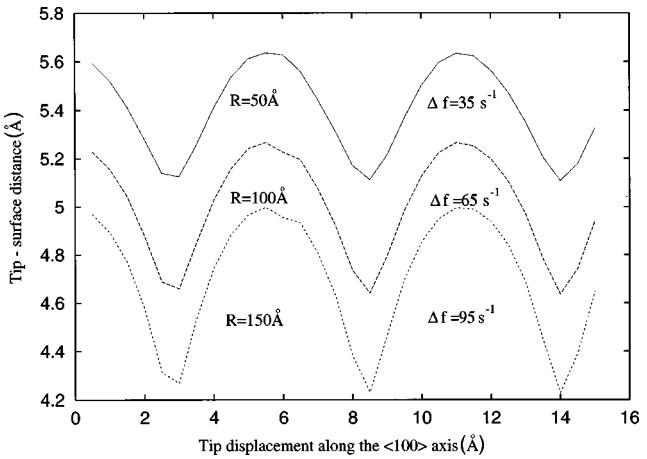

FIG. 5. The scanlines calculated for the maximum frequency shift $(\Delta f)_{max}$ obtained at different macroscopic tip radii for the MgO tip interaction with the NaCl surface.

ponent of the interaction are shown in Fig. 3. The full force on the tip was calculated by summing up the forces acting from all the surface ions on the tip ions and adding the van der Waals contribution acting on the macroscopic part of the tip from the rest of the semi-infinite surface. The interpolation procedure was then applied to construct the smooth surface image shown in Fig. 7.

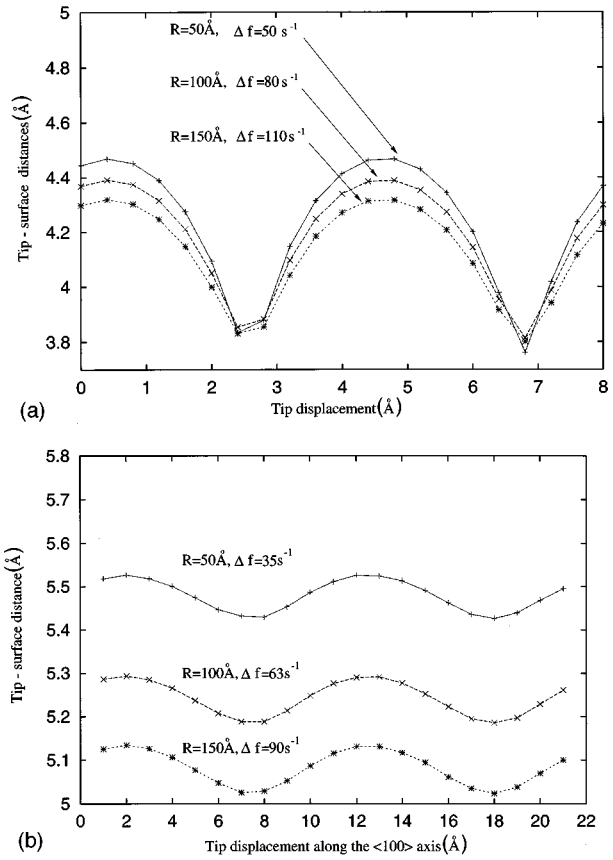

FIG. 6. The scanlines obtained for the MgO tip interaction with the MgO surface. (a) representative scanlines calculated at different microscopic tip radii and constant frequency shifts; (b) scanlines calculated for the same corrugation of 0.1 Å to study the dependence on the tip radius.

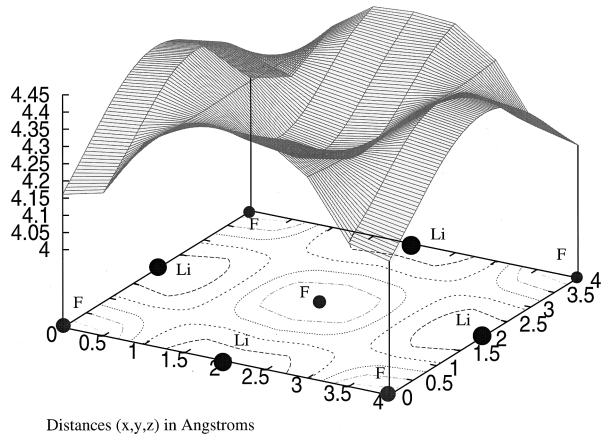

FIG. 7. The image of the LiF surface calculated using the force field obtained by the molecular dynamics technique with a tip radius of 50 Å and frequency shift $\Delta f = 45$ Hz.

C. Perfect surfaces

The contrast in the scanlines and in the surface image shown in Figs. 5–7 is determined by an interplay of the electrostatic and van der Waals forces. The main contributions to the contrast formation result from the interaction of the tip with the alternating surface potential and with the surface polarization induced by the electric field of the tip, i.e., by the same effect that causes instabilities of the surface and tip ions discussed in the previous section. The electrostatic potential of the MgO tip is shown in Fig. 2(f). If the tip is turned by its oxygen corner to the MgO surface, it attracts the Mg ions, which displace towards the tip, and repels the oxygen ions displacing them into the surface. Both displacements produce dipole moments that interact with the tip potential. The electrostatic potential of the MgO surface with one Mg ion displaced outwards by 0.15 Å is shown in Fig. 8. It was calculated using the same *ab initio* density-functional technique as was used in the tip calculations discussed in Sec. II. One can see that due to low coordination and high ionicity, the tip produces a strong localized potential that extends over several angstroms. The dipole potential of the displaced ion decays much slower than the exponentially decaying electrostatic potential of the ideal surface. Displacing ions outwards from the surface is easier than inwards. Out-

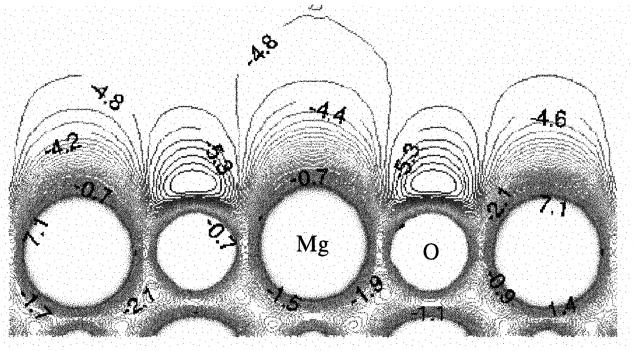

FIG. 8. Section of the electrostatic potential (in eV) produced by the MgO surface with one Mg ion displaced by 0.15 Å out from the surface.

ward displacement also increases the attraction due to the reduced distance to the tip. Therefore, the interaction of the tip with the induced lattice polarization above the cation and anion sites is different, which strongly contributes to the image contrast. If the tip moves closer, this finally leads to instability and strong displacement of the Li, Na, or Mg ions, as discussed above. In the case of LiF, this can be seen as the onset of strong attraction in the force curves in Fig. 3. This effect is also illustrated in Fig. 4, which shows the displacements of the surface Na ions at two positions of the MgO tip above the NaCl surface. One can see that the ''blunter'' tip used in these calculations causes strong displacements of both surface cations and anions, which are attracted to the oxygen and magnesium ions on the tip. Since MgO is much harder than both LiF and NaCl, the displacements of the MgO surface ions due to the interaction with the MgO tip are much smaller. In particular, the typical outward displacements of Mg ions were 0.07 Å and the inward displacements of O ions were 0.03 Å. Note that these displacements have opposite direction to the surface rumpling (about 0.02 Å in MgO). However, the ionic charges are twice as large and on balance the tip-surface interaction is not much different from that for LiF and NaCl. This discussion applies equally to the tip ions; however, their displacements in our case are much smaller than those for the softer NaCl surface. Finally, we should note that the contrast will inverse if the tip probes the surface by a positive low-coordinated ion.

Polarization of the surface ions by the electric field of the tip also contributes to the image contrast due to the different polarizability of cations and anions. This effect is accounted for in our MARVIN calculations for NaCl and MgO, but it is relatively small due to the small ion polarizabilities in these systems. Another factor which affects the contrast is the relationship between the surface interionic spacing and the effective diameter of the region where the tip has a strong electric field gradient which probes the surface (see Fig. 2). Roughly speaking, the tip can ''resolve'' the surface ions better if they are further apart. The difference this makes in our calculations is evident in the NaCl calculations, where the interionic spacing is about 1.4 times larger than in LiF and MgO. As one can see in Fig. 3, the interaction of the MgO tip with the LiF surface up to 4 Å is always attractive. However, for NaCl, the force curves above the surface chlorine ions are already repulsive when the tip is closer to the surface than approximately 4.5 Å.[19] This is because the direct Coulomb repulsion of the surface anions from the oxygen tip is not overcompensated by the attraction due the surface polarization, as takes place in LiF. This effect also determines the tip-surface distance range where one could expect a resolved image: the force curves above different surface sites split starting from approximately 5.5 Å for LiF, but for NaCl this distance is much larger—approximately 6.5 Å.

Let us return to a comparison of the scanlines in Figs. 5–7. Note that the maxima in the scanlines correspond to the areas of the strongest tip-surface attraction. For all the crystal surfaces studied, the scanline extrema correspond to the lattice positions of the surface ions. As discussed above, for the given force field $F(x,y,z)$ and parameters of cantilever oscillations f_0 and A_1, the corrugation and other features of scanlines depend on two parameters: (i) the strength of the ''macroscopic part'' of the van der Waals interaction (determined by the tip radius R), and (ii) the frequency shift Δf. It is known that an attractive tip-surface interaction decreases the frequency of cantilever oscillations whereas a repulsive interaction makes it bigger than f_0. Therefore, in the presence of repulsion, as is the case in NaCl, there is a maximum frequency shift $(\Delta f)_{\max}$ corresponding to the maximum attraction before the frequency starts to increase thus decreasing Δf. To estimate the maximum scanline corrugation at given cantilever and interaction parameters, we calculated the scanlines for the NaCl surface at the frequency change $(\Delta f)_{\max}$ for three different effective tip radii (see Fig. 5). One can see that as the van der Waals interaction increases, the tip moves closer to the surface and both the $(\Delta f)_{\max}$ and the scanline corrugation become bigger.

In the cases of LiF and MgO, the distance range used in the force-field calculations was restricted by the critical distance (about 3.8 Å) for instabilities of the surface ions and did not reach the repulsive part of the interaction. Comparing the scanline for NaCl with the LiF image for the close parameters $R=50$ Å and $\Delta f=35$ Hz (see Fig. 7), we note that the LiF image has a smaller corrugation and is obtained 1 Å closer to the surface. This reflects the fact that since LiF has a much smaller interionic distance, the tip has to move closer in order to ''resolve'' different ions.

The Hamaker constant for the interaction of the MgO tip with the MgO surface is roughly twice that for NaCl.[69] Therefore, at the same tip radius and tip-surface distance range, the van der Waals interaction is also stronger and increases more rapidly as the tip moves closer to the surface. However, the difference in the chemical interaction between cation and anion sites of MgO is still small even at 5 Å. This results from the hardness and small interionic distance of MgO. As a result, one needs to move the tip closer to the surface in order to obtain the same corrugation as in NaCl. At the distance range about 3.8–4.5 Å, the maximum corrugation obtained in our calculations is about 0.6 Å.

A relevant question is how does the sensitivity of the technique depend on the tip radius? To give a qualitative answer to this question, we took as a criterion of sensitivity a minimum scanline corrugation of 0.1 Å and considered the interaction of tips with three different radii with the MgO surface. The results shown in Fig. 6(b) demonstrate that, in order to obtain the same scanline corrugation, with a blunter tip one should use a much larger frequency shift and move closer to the surface than with the sharper tip. In other words, sharp tips are better both in terms of sensitivity and stability of NC-SFM operation. This results from the fact that corrugation is determined by the relative changes of the force in the lateral direction. As the van der Waals interaction increases, the relative changes of the force at the same tip height, determined by the chemical contribution, decrease. Therefore the tip should move closer to the surface where the split of the force curves is larger; this increases both the scanline corrugation and the frequency shift.

The experimental images, and especially the observation of several point defects have raised expectations that NC-SFM is capable of obtaining ''true'' atomic resolution.[6,16] The results of this paper essentially confirm these expectations and demonstrate that periodic images in NC-SFM reflect the periodic arrangement of the surface ions. This ex-

perimental achievement should allow us to study point defects at surfaces and therefore their identification in images is becoming an important issue.

D. Point defects

To study what a simple point defect would look like in a NC-SFM image, we have calculated an image of a Mg^{2+} impurity ion compensated by a cation vacancy on the surface of LiF using the molecular-dynamics technique. The structure and stability of this defect has been studied in our previous publication[27] using the MARVIN code and the same set of potential parameters are used here. These calculations have demonstrated that the most stable defect configuration is where the Mg^{2+} ion is located in the plane just below the (001) surface plane and the compensating vacancy is in the surface plane. The energy difference between that configuration and the one where both the impurity and the vacancy are in the surface plane is about 0.3 eV. The cation vacancy is much more mobile at the surface than in the bulk: the calculated adiabatic barrier for the vacancy jumps around the impurity ion in the surface plane is 0.36 eV. The calculated and experimentally measured[70] barrier for these jumps in the bulk is about 0.7 eV. The impurity ion can diffuse by exchanging places with the vacancy. The calculated barrier for this exchange in the surface plane is equal to 1.3 eV.[27] These results suggest that the Mg^{2+} ion may stay at its site for a period that is much longer than required for taking an NC-SFM image (several seconds). Using the Vineyard theory it was estimated[27] that the cation vacancy at room temperature will jump to another equivalent site near the Mg^{2+} ion approximately every microsecond. This time is shorter than or comparable to the typical period NC-SFM cantilever oscillations ($f_0 = 100-300$ kHz). Therefore, at room temperature, the image will be averaged over many vacancy jumps. Although how to simulate averaging and construct an image under these conditions is clearly an important issue, this is beyond the scope of this paper. The vacancy jumps will be frozen for more than a minute if the surface temperature drops down about 180 K. Therefore, since low-temperature NC-SFM's are becoming increasingly available,[18] it is not unrealistic to assume a particular defect configuration for the period of scanning. Therefore, we focus on the image contrast for the static defect located in the surface plane in further discussion.

Recently, we performed a molecular-dynamics simulation which clearly demonstrated that contact SFM is very likely to modify or completely destroy the Mg^{2+}-vacancy defect during scanning.[71] The results of the present calculations give a more optimistic picture. The defect image shown in Fig. 9 was constructed on the basis of the force field calculated on the mesh including 91 surface points and the technique described above. The tip parameters were the same as in Fig. 7 and $\Delta f = 45$ Hz. It can be seen that the defect image at these parameters corresponds to a much larger tip-surface separation than for the perfect surface. In terms of color contrast used in experimental images, it looks like a wide bright spot that covers an area of several interionic spacings and a smaller dark spot at the vacancy position. The image looks this way mainly because the interaction between the tip and the vacancy is much weaker than with the impurity ion and

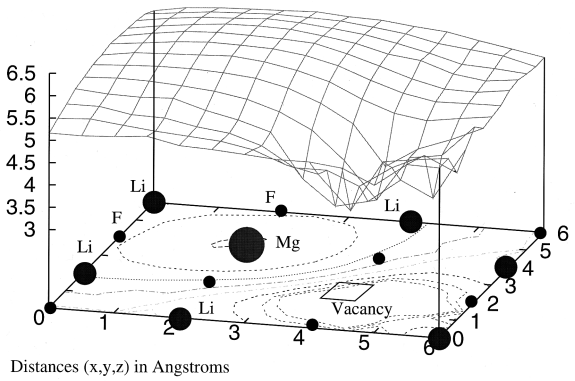

FIG. 9. The image of the Mg^{2+}-cation vacancy defect calculated using the force field obtained by the molecular-dynamics technique at a tip radius of 50 Å and a frequency shift $\Delta f = 45$ Hz.

becomes repulsive above the vacancy at approximately 4.3 Å due to repulsion of the tip oxygen ion from four surface fluorines surrounding the vacancy.[27] Therefore the tip must move higher if it's not to crash into the vacancy.

V. DISCUSSION

The mechanism of contrast formation in NC-SFM imaging of ionic surfaces found in this paper is based on the interplay between the electrostatic and the van der Waals interaction. The main contributions to electrostatics are the tip interaction with the surface Madelung potential and with the local surface polarization induced by the tip. Our results clearly demonstrate that the site dependence of the tip-induced surface relaxation determines the surface polarization and strongly contributes to the contrast formation. As was suggested in Ref. 5, this effect may also take place in NC-SFM imaging of Si(111). This is also supported by the early calculations by Abraham, Batra, and Ciraci[72] which have demonstrated the importance of surface relaxation in the SFM imaging of the Si surface in the contact mode.

The strength of the electrostatic interaction is determined by the local electric field of the tip. In our model, this field is produced by the low-coordinated site at the surface of ionic tip. The first question to ask is how realistic is this tip model and does it have any relation to SFM experiments? As we have demonstrated in Sec. II, although the MgO tip is never used experimentally, it represents a certain class of polar tips. These may include commercial tips which have a native oxide layer or a residual oxide left after bombardment with Ar ions. Oxygen or other ions can also be adsorbed on Si or metallic tips after accidental contact with surfaces during scanning.

The only criterion of correctness of our model is comparison with the experimental scanlines. The average scanline corrugations reported for several alkali halides[16] at a Δf of approximately 70 Hz are in the limits of 0.5–1.5 Å. Our modeling gives the values of 0.3–0.7 Å. A maximum corrugation of approximately 1.0 Å can be obtained for the NaCl surface at larger tip radii than shown in Fig. 5. Thus, for realistic tip parameters, the results of our calculations give the corrugations which are close to average experimental values.[16] A more covalent tip, such as pure Si, will experience polarization by the surface potential,[50] but we would

expect a much smaller image contrast due to this interaction.

As discussed above, the stability of NC-SFM operation is an important issue because both fluctuations in the tip oscillation amplitude and the effects like avalanche adhesion may lead to the tip poking into the surface and its modification. Our results suggest that the tip-surface distance range of contrast imaging for our tip model is approximately 4.0–6.0 Å. The lower limit is determined by the avalanche adhesion of surface ions onto the tip. It is interesting to note that the critical distance of approximately 4.0 Å is characteristic to very different pairs of materials.[26,28,51,65,67] It corresponds approximately to two times the interatomic distance, which is easy to understand in simple cases, such as considered in, e.g., Refs. 51 and 66. Our analysis of the possible causes of instabilities of NC-SFM indicates that this technique is not a clear-cut noninvasive surface probe. Adhesion of the surface ions and especially of charged impurities in the surface layer to the tip may lead to the tip and surface modification, image inversion and difficulties in identification of surface defects.

One of the shortcomings of SFM is that all the information about the system is contained in the force measurements, which are then transformed into a structural image. The combination of noncontact SFM with STM on thin insulating (especially oxide) films may provide a tool that may yield more information about the system and make the interpretation of the results more reliable.

ACKNOWLEDGMENTS

A.I.L. and A.S.F. would like to acknowledge the EPSRC, and A.L.R. the Australian Government's Cooperative Research Centre Program, for financial support. The authors are grateful to F. J. Giessibl, A. Baratoff, R. Bennewitz, E. Meyer, and all members of the Basel SPM group for very useful and stimulating discussions on NC-SFM, and to G. Thornton and H. Raza for illuminating comments on applications of NC-SFM to oxides. We would like to thank J. Gavartin for introducing us to the world of Si clusters, R. Pérez for providing the LDA optimized structure of the Si(111) (5×5) reconstruction, and P. Sushko and L. Kantorovich for help in calculations and many useful discussions. We would like to thank G. Kresse for his help with the VASP code. We are grateful for an allocation of time on Cray T3E at EPCC provided by the High Performance Computing Initiative through the Materials Chemistry consortium.

[1] F. J. Giessibl, Jpn. J. Appl. Phys., Part 1 **33**, 3726 (1994).
[2] F. J. Giessibl, Science **267**, 68 (1995).
[3] R. Lüthi, E. Meyer, M. Bammerlin, A. Baratoff, T. Lehmann, L. Howald, C. Gerber, and H.-J. Güntherodt, Z. Phys. B **100**, 165 (1996).
[4] Y. Sugawara, M. Ohta, H. Ueyama, S. Morita, F. Osaka, S. Ohkouchi, M. Suzuki, and S. Mishima, J. Vac. Sci. Technol. B **14**, 953 (1996).
[5] R. Erlandsson, L. Olsson, and P. Mårtensson, Phys. Rev. B **54**, R8309 (1996).
[6] M. Bammerlin, R. Lüthi, E. Meyer, A. Baratoff, J. Lu, M. Guggisberg, C. Gerber, L. Howald, and H.-J. Güntherodt, Probe Microscopy **1**, 3 (1997).
[7] U. Dürig, J. K. Gimzewski, and D. W. Pohl, Phys. Rev. Lett. **57**, 2403 (1986).
[8] Y. Martin, C. C. Williams, and H. K. Wickramasighe, J. Appl. Phys. **61**, 4723 (1987).
[9] U. Dürig, O. Züger, and A. Stalder, J. Appl. Phys. **72**, 1778 (1992).
[10] N. A. Burnham, O. P. Behrend, F. Oulevey, G. Gremaud, P.-J. Gallo, D. Gourdon, E. Dupas, A. J. Kulik, H. M. Pollock, and G. A. D. Briggs, Nanotechnology **8**, 67 (1997).
[11] D. Krüger, B. Anczykowski, and H. Fuchs, Ann. Phys. (Leipzig) **6**, 341 (1997).
[12] S. P. Jarvis, H. Yamada, S.-I. Yamamoto, H. Tokumoto, and J. B. Pethica, Nature (London) **384**, 247 (1996).
[13] U. Dürig, H. R. Steinauer, and N. Blanc, J. Appl. Phys. **82**, 3641 (1997).
[14] F. J. Giessibl and M. Tortonese, Appl. Phys. Lett. **70**, 2529 (1997).
[15] K. Fukui, H. Onishi, and Y. Iwasawa, Phys. Rev. Lett. **79**, 4202 (1997).
[16] M. Bammerlin, R. Lüthi, E. Meyer, A. Baratoff, M. Guggisberg, C. Loppacher, J. Lu, C. Gerber, and H.-J. Güntherodt, Appl. Phys. A: Mater. Sci. Process. **66**, S293 (1998).
[17] F. J. Giessibl, Phys. Rev. B **56**, 16 010 (1997).
[18] W. Allers, A. Schwarz, U. D. Schwarz, and R. Wiesendanger, Rev. Sci. Instrum. **69**, 221 (1998).
[19] A. I. Livshits, A. L. Shluger, and A. L. Rohl, Appl. Surf. Sci. (to be published March 1999).
[20] P. Gleyzes, P. K. Kuo, and A. C. Boccara, Appl. Phys. Lett. **58**, 2989 (1991).
[21] R. G. Winkler, J. P. Spatz, S. Sheiko, M. Möller, P. Reineker, and O. Marti, Phys. Rev. B **54**, 8908 (1996).
[22] R. Pérez, M. C. Payne, I. Stich, and K. Terakura, Phys. Rev. Lett. **78**, 678 (1997).
[23] I. Y. Sokolov, G. S. Henderson, and F. J. Wicks, Surf. Sci. **381**, L558 (1997).
[24] J. B. Pethica and A. P. Sutton, J. Vac. Sci. Technol. A **6**, 2490 (1988).
[25] J. R. Smith, G. Bozzolo, A. Banerjea, and J. Ferrante, Phys. Rev. Lett. **63**, 1269 (1989).
[26] U. Landman, W. D. Luedtke, N. A. Burnham, and R. J. Colton, Science **248**, 454 (1990).
[27] A. L. Shluger, A. L. Rohl, D. H. Gay, and R. T. Williams, J. Phys.: Condens. Matter **6**, 1825 (1994).
[28] A. L. Shluger, L. N. Kantorovich, A. I. Livshits, and M. J. Gillan, Phys. Rev. B **56**, 15 332 (1997).
[29] A. L. Shluger, A. L. Rohl, R. T. Williams, and R. M. Wilson, Phys. Rev. B **52**, 11 398 (1995).
[30] A. I. Livshits and A. L. Shluger, Faraday Discuss. **106**, 425 (1997).
[31] A. I. Livshits and A. L. Shluger, Phys. Rev. B **56**, 12 482 (1997).
[32] F. J. Giessibl and G. Binnig, Ultramicroscopy **42-44**, 281 (1992).
[33] L. Howald, H. Haefke, R. Lüthi, E. Mayer, G. Gerth, H. Rudin, and H.-J. Güntherodt, Phys. Rev. B **49**, 5651 (1994).
[34] D. V. Labeke, B. Labani, and C. Girard, Chem. Phys. Lett. **162**, 399 (1989).

[35] J. N. Israelachvili, *Intermolecular and Surface Forces* (Academic, London, 1991).
[36] C. Argento and R. H. French, J. Appl. Phys. **80**, 6081 (1996).
[37] P. V. Sushko, A. S. Foster, L. N. Kantorovich, and A. L. Shluger, Appl. Surf. Sci. (to be published April 1999).
[38] R. Car and M. Parrinello, Phys. Rev. Lett. **55**, 2471 (1985).
[39] G. Kresse and J. Furthmuller, Phys. Rev. B **54**, 11 169 (1996).
[40] G. Kresse and J. Furthmuller, Comput. Mater. Sci. **6**, 15 (1996).
[41] D. Vanderbilt, Phys. Rev. B **41**, 7892 (1990).
[42] K. Laasonen, A. Pasquarello, R. Car, C. Lee, and D. Vanderbilt, Phys. Rev. B **47**, 10 142 (1993).
[43] J. P. Perdew, in *Electronic Structure in Solids' 91*, edited by P. Ziesche and H. Eschrig (Academie Verlag, Berlin, 1991).
[44] J. P. Perdew, J. A. Chevary, S. H. Vosko, K. A. Jackson, M. R. Pederson, D. J. Singh, and C. Fiolhais, Phys. Rev. B **46**, 6671 (1992).
[45] E. Kaxiras, Phys. Rev. Lett. **64**, 551 (1990).
[46] M. Krack and K. Jug, Chem. Phys. **192**, 127 (1995).
[47] K. Takayanagi, Y. Tanishiro, M. Takahashi, and S. Takahashi, J. Vac. Sci. Technol. A **3**, 1502 (1981).
[48] M. A. Zaibi, J. P. Lacharme, and C. A. Sebenne, Surf. Sci. **377**, 639 (1997).
[49] C. Pancey, F. Rochet, G. Dufour, A. Roulet, F. Sirotti, and E. Panaccione, Surf. Sci. **338**, 143 (1995).
[50] F. J. Giessibl, Phys. Rev. B **45**, 13 815 (1992).
[51] S. Ciraci, E. Tekman, and A. Baratoff, Phys. Rev. B **46**, 10 411 (1992).
[52] N. A. Burnham, R. J. Colton, and H. M. Pollock, Nanotechnology **4**, 64 (1993).
[53] U. Hartmann, Adv. Electron. Electron Phys. **87**, 49 (1994).
[54] A. L. Shluger and A. L. Rohl, Top. Catal. **3**, 221 (1996).
[55] D. H. Gay and A. L. Rohl, J. Chem. Soc., Faraday Trans. **91**, 925 (1995).
[56] P. W. Tasker, Philos. Mag. A **39**, 119 (1979).
[57] B. G. Dick and A. W. Overhauser, Phys. Rev. **112**, 90 (1958).
[58] D. M. Heyes, M. Barber, and J. H. R. Clarke, J. Chem. Soc., Faraday Trans. 2 **73**, 1485 (1977).
[59] R. W. Grimes, C. R. A. Catlow, and A. M. Stoneham, J. Phys.: Condens. Matter **1**, 7367 (1989).
[60] D. J. Binks, Ph.D. thesis, University of Surrey, 1994.
[61] DL_POLY is a package of molecular simulation routines written by W. Smith and T. R. Forester, Copyright: the EPSRC acting through its Daresbury and Rutherford Appleton Laboratory at Daresbury Laboratory, 1994.
[62] H. J. C. Berendsen, J. P. M. Posma, W. F. V. Gunsteren, A. D. Nola, and J. R. Haak, J. Chem. Phys. **81**, 3684 (1984).
[63] D. Tabor and R. H. S. Winterton, Proc. R. Soc. London, Ser. A **312**, 435 (1969).
[64] J. B. Pethica and A. P. Sutton, J. Vac. Sci. Technol. A **6**, 2490 (1988).
[65] U. Dürig, in *Forces in Scanning Probe Methods*, edited by H.-J. Güntherodt, D. Anselmetti, and E. Meyer (Kluwer, Dordrecht, 1995), p. 191.
[66] B. S. Good and A. Banerjea, J. Phys.: Condens. Matter **8**, 1325 (1996).
[67] M. R. Sørensen, K. W. Jacobsen, and H. Jónsson, Phys. Rev. Lett. **77**, 5067 (1996).
[68] U. Landman, W. D. Luedtke, and E. M. Ringer, Wear **153**, 3 (1992).
[69] R. H. French, R. M. Cannon, L. K. DeNoyer, and Y.-M. Chiang, Solid State Ionics **75**, 13 (1995).
[70] J. S. Dryden and R. J. Meakins, Discuss. Faraday Soc. **23**, 39 (1957).
[71] A. I. Livshits and A. L. Shluger, Appl. Surf. Sci. (to be published February 1999).
[72] F. A. Abraham, I. P. Batra, and S. Ciraci, Phys. Rev. Lett. **60**, 1314 (1988).